



Article

# In-Situ AFM Studies of Surfactant Adsorption on Stainless Steel Surfaces during Electrochemical Polarization

Julian Cremer <sup>1,\*</sup> , Sinan Kiremit <sup>2,3</sup>, Heinz Jürgen Klarhorst <sup>2</sup>, Alix Gaspard <sup>4</sup>, Karsten Rasim <sup>4</sup>, Thomas Kordisch <sup>2</sup> , Andreas Hütten <sup>3</sup> and Dario Anselmetti <sup>1,\*</sup>

<sup>1</sup> Department of Experimental Biophysics & Applied Nanoscience, Faculty of Physics, Bielefeld University, 33615 Bielefeld, Germany

<sup>2</sup> Bielefeld Institute for Applied Materials Research, Faculty of Engineering and Mathematics, Hochschule Bielefeld University of Applied Sciences and Arts, Interaktion 1, 33619 Bielefeld, Germany; thomas.kordisch@hsbi.de (T.K.)

<sup>3</sup> Department of Thin Films and Physics of Nanostructures, Center of Spinelectronic Materials and Devices, Faculty of Physics, Bielefeld University, 33615 Bielefeld, Germany; andreas.huetten@uni-bielefeld.de

<sup>4</sup> Center for Materials, Business Unit Laundry, R&D, Miele & Cie. KG, 33332 Gütersloh, Germany; karsten.rasim@miele.com (K.R.)

\* Correspondence: jcremer@physik.uni-bielefeld.de (J.C.); dario.anselmetti@physik.uni-bielefeld.de (D.A.)

**Abstract:** Corrosion inhibitors are one of the best practices to prevent the far-reaching negative impacts of corrosion on ferrous alloys. A thorough understanding of their corrosion-inhibiting effects is essential for a sustainable economy and environment. Anionic surfactants are known to act efficiently as corrosion inhibitors. Here, we present that in-situ atomic force microscopy (AFM) measurements can provide deep insights into the adsorption and inhibition mechanism of surfactants on stainless steel surfaces during local corrosion. These include the configuration of surfactant molecules on the surface and how the microstructure of the stainless steel surface influences the inhibition process. Three different anionic surfactants, namely palm kernel oil (PKO), linear alkylbenzene sulfonate (LAS), and fatty alcohol ether sulfate (FAES), were investigated on a titanium-stabilized ferritic stainless steel (1.4510) in NaCl solution. For PKO, the results show random adsorption of bi- and multilayer whereas LAS and FAES adsorb only as local corrosion occurs. Thereby, LAS accumulates only locally and especially at the titanium precipitates of the 1.4510 and FAES forms a densely packed monolayer on the surface. This leads to better corrosion inhibiting properties for LAS and FAES compared to PKO.

**Keywords:** AFM; adsorption; aggregation; corrosion; corrosion inhibitors; surfactants; stainless steel



**Citation:** Cremer, J.; Kiremit, S.; Klarhorst, H.J.; Gaspard, A.; Rasim, K.; Kordisch, T.; Hütten, A.; Anselmetti, D. In-Situ AFM Studies of Surfactant Adsorption on Stainless Steel Surfaces during Electrochemical Polarization. *Corros. Mater. Degrad.* **2024**, *5*, 224–240. <https://doi.org/10.3390/cmd5020009>

Academic Editor: Angeliki G. Lekatou

Received: 16 February 2024

Revised: 19 March 2024

Accepted: 29 March 2024

Published: 7 April 2024



**Copyright:** © 2024 by the authors. Licensee MDPI, Basel, Switzerland. This article is an open access article distributed under the terms and conditions of the Creative Commons Attribution (CC BY) license (<https://creativecommons.org/licenses/by/4.0/>).

## 1. Introduction

Severe damage from corrosion occurs in nearly all industries worldwide [1,2]. Many stainless steels already exhibit high corrosion resistance due to their inherent chromium oxide layer [3–5]. However, the decisive factor for the necessary material properties and the required corrosion resistance is always the environment in which a steel is used [4–6]. Often, the presence of chloride ions poses a significant challenge, as they are known to damage the chromium oxide layer leading to pitting corrosion [4–6]. Environmentally friendly corrosion inhibitors such as surfactants offer the possibility to protect steel against harsh environments and thus significantly extend its service life [7–9]. Nevertheless, the protective nature of inhibitors needs to be better understood to enable their targeted use for specific steel grades and their field of application.

Electrochemical impedance spectroscopy (EIS) or electrochemical polarization methods are powerful tools to determine the corrosion resistance of a steel sample as well as the inhibition efficiency of a corrosion inhibitor in different solutions [8,10,11]. However, the measured values are always averaged over the entire steel surface. Consequently,

these measurement methods do not provide direct access to local effects that occur on the steel surface. This includes the assembly in which layer-forming inhibitors adhere to the surface, i.e., whether monolayers, bilayers or multilayers are formed, and how adsorption is affected by precipitates on the surface. In particular, precipitates such as titanium carbon-nitrides, chromium carbides, or manganese sulphides play a vital role because they are defects in the chromium oxide layer and may represent nucleation sites for pitting corrosion [12–14]. Furthermore, it is difficult to analyse the mode of action of the inhibitors when local corrosion occurs.

Anionic surfactants are the main ingredients in detergents and therefore washing active substances [15], but they are also known for their corrosion inhibiting properties [7–9]. The chemical and physical properties of these molecules are determined by their negatively charged hydrophilic head group and hydrophobic alkyl tail. Surfactants are typically classified as mixed inhibitors, i.e., they act as both anodic and cathodic inhibitors, since they ought to provide corrosion protection by surface coverage [8,9,16]. Adsorption is generally possible by physisorption or chemisorption. In physisorption, the head group of the surfactant interacts with the steel surface via electrostatic or van der Waal interactions. Chemisorption results in a chemical bond between the surfactant and the steel, typically with a coordinative bond between organic heteroatoms of the head group and the iron [8,9,16]. In addition to the interaction of the head group with the steel surface, the aggregation properties of the surfactants are also important for the adsorption, which can be quantified by the critical micelle concentration (CMC) [17,18]. A surfactant that aggregates or adsorbs even at low concentrations is typically desirable.

Only a few scientific studies have been reported on surfactants that do not initially adsorb on stainless steel surfaces [19,20]. Yalcinkakya et al. [20] and Tobsin et al. [19] obtained significantly higher pitting potentials with surfactants at nearly constant effective capacitance or corrosion current. It can be concluded that, in these cases, the inhibition is not due to the formation of a protective layer during immersion and therefore another inhibition mechanism must be present, which remains to be elucidated. In this paper, we demonstrate that electrochemical polarization measurements in an AFM liquid cell allow imaging of the stainless steel surface before and after local corrosion, revealing surface effects at a resolution down to molecular adsorption. The different adsorption behavior of palm kernel oil (PKO), linear alkylbenzene sulfonate (LAS), and fatty alcohol ether sulfate (FAES) PKO were investigated on a 1.4510 stainless steel in NaCl solution. The critical micelle concentration and headgroup area were determined by surface tension measurements to quantify the aggregation of surfactant molecules. Potentiodynamic polarization measurements associated with the in-situ atomic force microscopy (AFM) results are presented and compared with respect to the inhibition efficiency. Based on these results, the different inhibition mechanisms of the three surfactants can be demonstrated.

## 2. Materials and Methods

### 2.1. Materials

The chemical composition of the titanium-stabilized 1.4510 (X3CrTi17, AISI 439) was determined by optical emission spectroscopy (LAB S, SPECTRO Analytical Instruments GmbH, Kleve, Germany) and is listed in Table 1 [21]. The stainless steel was received as cold-rolled and annealed 0.5 mm thick sheets. Samples for electrochemical and in-situ AFM measurements were water-jet cut, ground with SiC (grid size 15.3  $\mu\text{m}$ ) and diamond suspensions (grid size 9  $\mu\text{m}$ , 3  $\mu\text{m}$  and 1  $\mu\text{m}$ ), and polished with colloidal silica (grain size 0.06  $\mu\text{m}$ ) using a Bühler Phoenix 4000 (Apeldoorn, The Netherlands) polishing machine.

**Table 1.** Chemical composition of the stainless steel 1.4510.

	C	N	Si	Mn	P	Cr	Ti	Ni	Mo	S	Fe
wt.%	0.02	0.02	0.44	0.41	0.03	16.00	0.37	0.17	0.03	<0.001	bal.

The chemical structure of the three investigated anionic surfactants is depicted in Figure 1. The lengths of the alkyl hydrocarbon chains are C12–18 for the palm kernel oil (PKO) (CAS 90990-15-1), C10–13 for the linear alkylbenzene sulfonate (LAS) (CAS 85536-14-7), and C12–14 for the fatty alcohol ether sulfate (FAES) (CAS 68891-38-3). Depending on the chain length and the number of ether groups in FAES, the molar masses are in the range of  $M_{\text{PKO}} = 214\text{--}299$  g/mol,  $M_{\text{LAS}} = 320\text{--}363$  g/mol, and  $M_{\text{FAES}} = 332\text{--}484$  g/mol. The surfactants, purchased from Dalli Group, were received in a neutralized state (with NaOH) with a pH of 8.1 for LAS and FAES and a pH of 8.3 for the PKO.

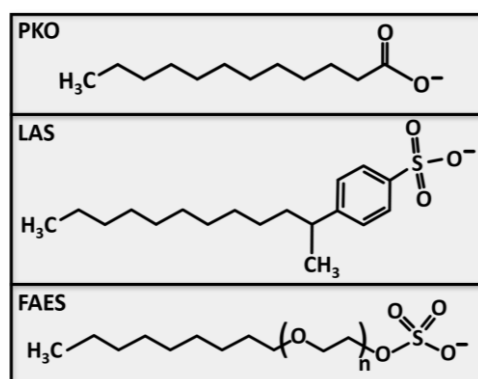


**Figure 1.** Structural formula of the anionic surfactants palm kernel oil (PKO), linear alkylbenzene sulfonate (LAS) and fatty alcohol ether sulfate (FAES).

## 2.2. Measurement Methods

### 2.2.1. Force Tensiometer

The critical micelle concentration was determined by surface tension measurements using a DCAT 21 force tensiometer from DataPhysics Instruments (Charlotte, NC, USA) with a Wilhelmy Plate (l: 10 mm, w: 19.9 mm and t: 0.2 mm). Immersion speed was 1 mm/s and immersion depth 3 mm. The solution consisted of NaCl with 500 mg/L Cl<sup>-</sup> and a pH of 5.9 prepared with distilled water and was tempered to 30 °C during the measurement. The surface tension was recorded as a function of surfactant concentration to determine the critical micelle concentration and head group area of each molecule.

### 2.2.2. Electrochemical Polarization

An electrochemical corrosion cell with a standard three-electrode setup was used, consisting of a working electrode (WE), a counter electrode (CE), and a reference electrode (RE). The 1.4510 steel sample functioned as the WE with a test area of 1 cm<sup>2</sup>. The test area was confined with a round electrochemical mask (3M model 470 electroplater's tape). The CE was made of platinized titanium and the RE was a silver/silver chloride (Ag/AgCl) immersed in 3 mol/L potassium chloride (KCl) solution of a Haber-Luggin capillary with a potential difference of +207 mV referred to a standard hydrogen electrode. A beaker containing 800 mL of NaCl solution with a concentration of 500 mg/L Cl<sup>-</sup> (pH 5.9) was used with a laboratory heat plate to keep the temperature at 30 °C. The test solution was not deaerated to establish an application-oriented environment characteristic of surfactant inhibition, as encountered in settings like a washing machine. The measurements were recorded for different concentrations of surfactant in the NaCl solution with a MLab100 potentiostat (Bank Elektronik–Intelligent Controls GmbH, Pohlheim, Germany). The open circuit potential was measured for 5 min before the potentiodynamic polarization was started from -400 mV vs. Ag/AgCl at a rate of 1 mV/s. The measurements were stopped when the current reached a value of 100 μA/cm<sup>2</sup>. Additionally, the Tafel extrapolation method was used to calculate the corrosion potential ( $E_{\text{corr}}$ ) and the corrosion current density ( $j_{\text{corr}}$ ). All measurements were carried out at least three times for each surfactant concentration. After electrochemical polarization, the stainless steel surfaces were examined

under a light microscope (Axioscope, Carl Zeiss AG, Oberkochen, Germany) to identify the occurrence of localized corrosion, i.e., pitting or crevice corrosion.

### 2.2.3. In-Situ Atomic Force Microscopy

The in-situ AFM measurements were performed with a NanoWizard™ UltraSpeed 2 AFM equipped with a heating cooling stage and an electrochemistry cell (JPK-Bruker, Berlin, Germany). The 1.4510 steel sample functioned as a working electrode with a test area of 1.8 cm<sup>2</sup>. The counter electrode consisted of a platinum wire and the Ag/AgCl reference electrode was a short Dri-Ref™ (World Precision Instruments, Sarasota, FL, USA) with a potential difference of +210 mV referred to a standard hydrogen electrode. The electrochemistry cell was filled with the NaCl solution (500 mg/L Cl<sup>-</sup> and pH 5.9) and one of the three surfactants. The electrochemical measurements were recorded at 30 °C with the same MLab 100 potentiostat as described before. The solution was not stirred during the measurement. AFM high resolution imaging was conducted simultaneously with DNP-10-A (Bruker, 0.35 N/m, 65 kHz) or USC-F0.3 (NanoWorld, 0.3 N/m, 300 kHz) cantilever in tapping mode. The experimental setup is shown in Figure 2.

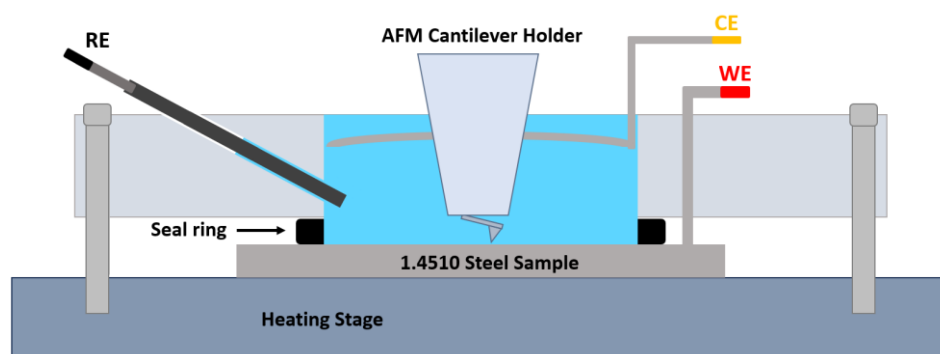


**Figure 2.** Sketch of temperature-controlled electrochemistry cell for in-situ AFM measurements filled with NaCl solution. WE, CE, and RE denote for 1.4510 steel sample, platinum wire, and Ag/AgCl electrode, respectively. The cantilever holder can be immersed in the solution with the measuring tip approaching the metal surface subsequently imaging it.

The measurements were carried out according to the following workflow. The NaCl surfactant solution was tempered at 30 °C for 10 min. Then the OCP was measured for 5 min and the tip was moved toward the surface. Initial images of the stainless steel surface at different locations were taken to pinpoint a titanium precipitate Ti(C,N) and to detect whether surfactants were adsorbed during immersion. The recorded AFM height image of the stainless steel surface in the NaCl-surfactant solution represents the initial state. Next, the tip was retracted 500 μm from the surface and a constant potential difference was applied. After 2 min, the tip was approached again and AFM height images at the same location were taken to record topographical changes like local corrosion or surfactant adhesion. If no topographical changes compared to the initial state were detectable, the tip was retracted 500 μm from the surface and the applied potential was increased by 100 or 200 mV. This process was repeated until the current no longer remained constant but increased significantly over time, indicating the occurrence of localized corrosion. To prevent the stainless steel surface from being covered by corrosion products, which would make further AFM measurements impossible, the voltage was then switched off. After the current increase, the sample surface was imaged again. The AFM data were evaluated with the freely available software Gwyddion 2.58 [22].

## 3. Results

To elucidate the relationship between surfactant adsorption and corrosion inhibition, critical micelle concentrations were determined, electrochemical polarization experiments

were conducted, and the corrosion behaviour was observed with in-situ atomic force microscopy (AFM).

### 3.1. Critical Micelle Concentration

When surfactants are introduced into an aqueous solution, they preferentially accumulate at the air-water interface due to their amphiphilic nature, which reduces surface tension. The critical micelle concentration (CMC) of a surfactant represents a threshold concentration. Increasing the amount of surfactant above this limit will preferably result in the formation of micelles rather than further aggregation at the solution surface. Therefore, the decrease in surface tension over surfactant concentration will stop or proceed considerably slower, hence showing a change in slope in the corresponding plots, which makes it an easy-to-detect value. Surfactants with a low CMC are well suited for a self-assembly process and tend to be more effective at reducing surface tension.

The results of the surface tension measurements in the NaCl solution (500 mg/L Cl<sup>-</sup> and pH 5.9) at 30 °C are presented in Table 2 and an exemplary measurement curve is shown in Figure 3 for LAS. The surface tension decreases with increasing LAS concentration. The inlay in Figure 3 shows the same plot with logarithmic scale and the linear fits resulting in a CMC of 0.45 g/L.

**Table 2.** Measured CMC, surface tension above CMC  $\sigma_{\text{CMC}}$ , and the surface area per molecule  $a_0$  for LAS, FAES, and PKO in NaCl solution (500 mg/L Cl<sup>-</sup> and pH 5.9) at 30 °C.

NaCl 500 mg/L Cl <sup>-</sup> 30 °C	LAS	FAES	PKO
CMC (g/L)	0.45 ± 0.02	0.17 ± 0.04	0.013 ± 0.007
$\sigma_{\text{CMC}}$ (mN/m)	31.4 ± 0.3	29.1 ± 0.4	31.1 ± 0.4
$a_0$ (nm <sup>2</sup> )	0.54 ± 0.04	0.35 ± 0.03	0.20 ± 0.03

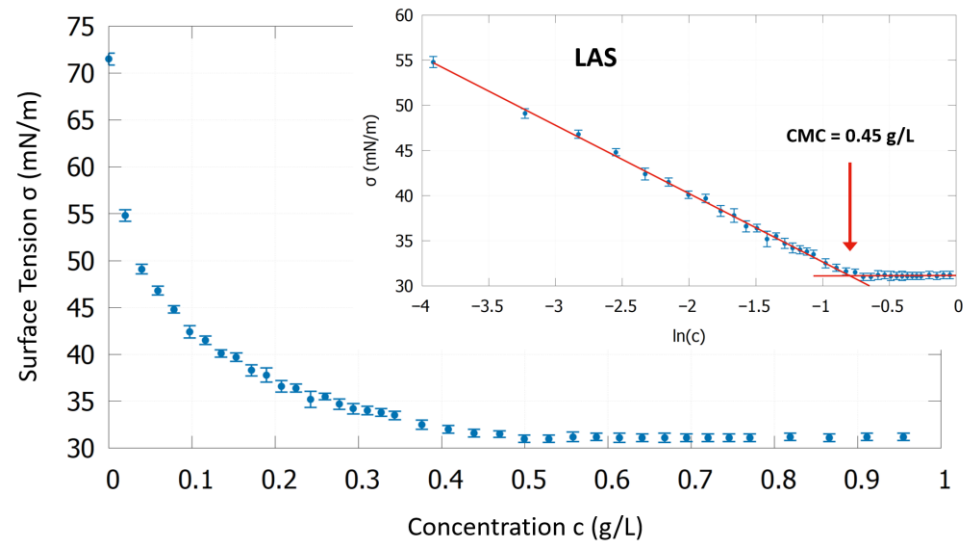


**Figure 3.** Measured surface tension as a function of LAS concentration in NaCl solution (500 mg/L Cl<sup>-</sup> and pH 5.9) at 30 °C. The inlay presents the same data with a logarithmic scale enabling linear fits to determine the CMC at the intersection.

The Gibbs isotherm relates the change in surface tension with the surface excess  $\Gamma$  and thereby the average area occupied by each single anionic surfactant molecule  $a_0$  at the water-air interface can be calculated [23]:

$$\Gamma = -\frac{1}{RT} \frac{\partial \sigma}{\partial \ln(c)} \quad (1)$$

$$a_0 = \frac{1}{N_A \Gamma} \quad (2)$$

with the universal gas constant  $R$ , the absolute temperature  $T$ , and the Avogadro constant  $N_A$ . Table 2 lists the CMC, the surface tension above the CMC  $\sigma_{\text{CMC}}$ , and the surface area per molecule  $a_0$  at the water/air interface for each of the three investigated surfactants.

PKO has by far the lowest CMC with 0.013 g/L, about 13 times smaller than FAES with 0.17 g/L. LAS has the highest CMC with 0.45 g/L. This order is also reflected in the surface area per molecule at the water/air interface. The surface tension decreases above the CMC a little further down to 29.1 mN/m for FAES compared to 31.4 mN/m for LAS and 31.1 mN/m for PKO.

### 3.2. Electrochemical Polarization

To quantify the inhibition efficiency of the three anionic surfactants and to gain first insight into the adsorption process, potentiodynamic polarization measurements were performed. The results are presented in Figure 4. Representative polarization curves are shown in Figure 4a for 1.4510 in NaCl solution (500 mg/L  $\text{Cl}^-$  and pH 5.9 at 30 °C), including one curve without surfactants and one curve for each of the three studied surfactants at  $8 \times \text{CMC}$ , respectively. The bar charts in Figure 4b–d show a summary of all results from the potentiodynamic measurements. The lower end of each bar is the mean value of the corrosion potential ( $E_{\text{corr}}$ ) and the upper end is the mean value of the pitting or crevice corrosion potential, depending on which occurred first. In the following it will be generally referred to as breakdown potential ( $E_{\text{bd}}$ ).

The stainless steel surfaces were examined under a light microscope after the electrochemical polarization to identify the occurrence of local corrosion (three specimens per surfactant concentration). We counted the pits and crevices (resolvable with a  $20 \times$  magnification) that had formed on each specimen. For each of the three surfactants examined, the number of pits tended to decrease, and the number of crevices tended to increase with surfactant concentration. The crevices always formed directly at the edge of the electrochemical mask. Calculating the relative frequency of pits  $\text{RF}_{\text{pit}}$  for each surfactant concentration, LAS and FAES appear to inhibit pitting corrosion more effectively than PKO (Figure 4e). With LAS, the  $\text{RF}_{\text{pit}}$  is less than 20% for  $4 \times \text{CMC}$  and higher concentrations. With FAES, the  $\text{RF}_{\text{pit}}$  is about 70% for  $4 \times \text{CMC}$  but also less than 20% for  $8 \times \text{CMC}$  and higher concentrations. With PKO, much higher concentrations are necessary to suppress pitting corrosion. The  $\text{RF}_{\text{pit}}$  decreases to 40% at  $40 \times \text{CMC}$  and does not decrease further for higher concentrations. This already indicates a different inhibitory mechanism of PKO compared with LAS and FAES. At the highest concentrations tested, LAS and FAES reached  $E_{\text{bd}}$  values of over 1300 mV; in some cases, this led to oxygen evolution, resulting in a rather uniform surface corrosion than a localized corrosion. Therefore, there are no  $\text{RF}_{\text{pit}}$  values for  $160 \times \text{CMC}$ .

All tested anionic surfactants act efficiently as corrosion inhibitors. The mean value of the pitting corrosion potential without surfactants was 403 mV for the 1.4510 in NaCl solution (500 mg/L  $\text{Cl}^-$  and pH 5.9 at 30 °C). This value is clearly exceeded by each of the three surfactants, even at low concentrations. The anodic breakdown potential  $E_{\text{bd}}$  in case of PKO reaches a limit for concentrations higher than  $20 \times \text{CMC}$ . For LAS, the  $E_{\text{bd}}$  no longer increases significantly above  $8 \times \text{CMC}$ . For FAES, the breakdown potential  $E_{\text{bd}}$  is constant in the range of  $2 \times \text{CMC}$  to  $8 \times \text{CMC}$  but continues to increase at higher FAES concentrations.

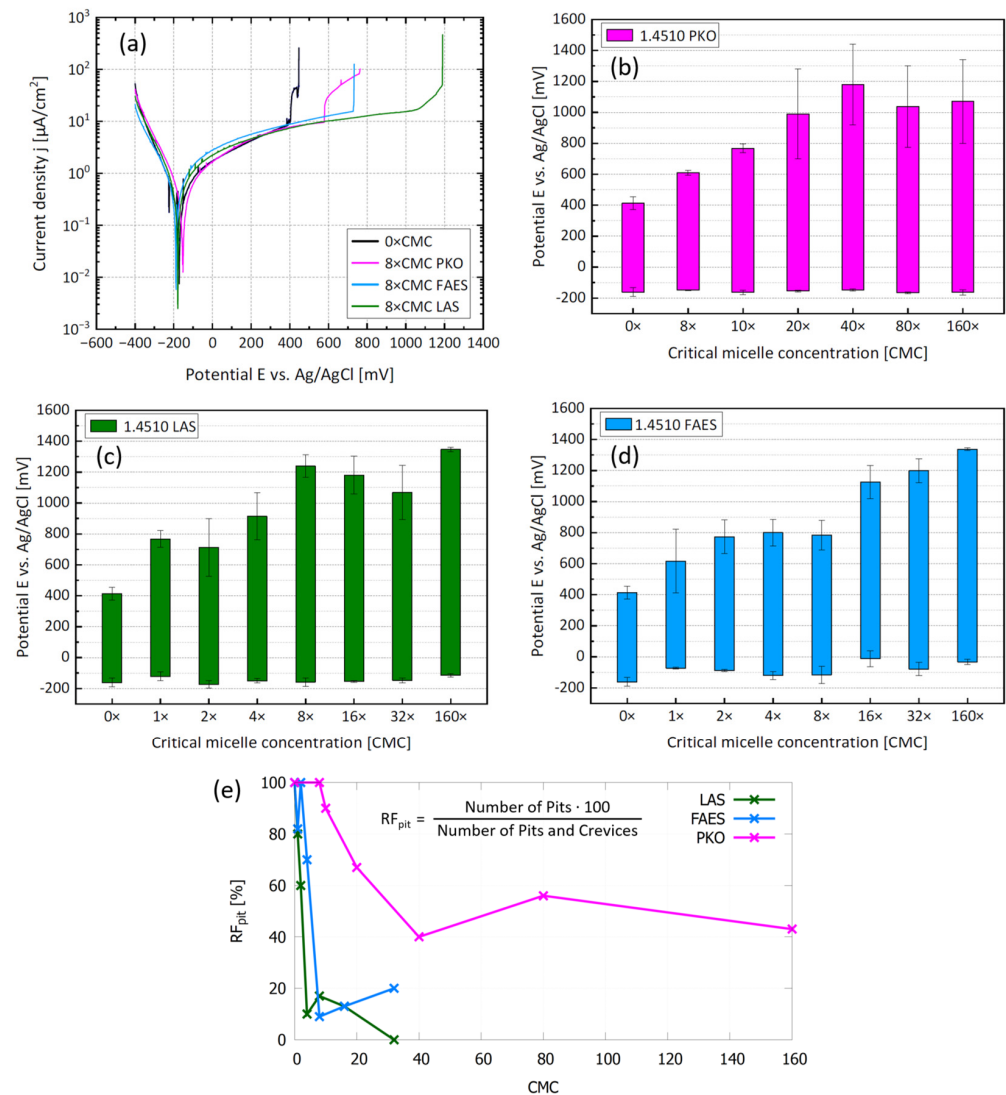


**Figure 4.** Potentiodynamic polarization results. (a) Typical polarization curves without and with surfactants. (b–d) Bars represent the passive region from the lower end = corrosion potential ( $E_{\text{corr}}$ ) to the upper end = anodic breakdown potential ( $E_{\text{bd}}$ ) for different concentrations of (b) PKO (c) LAS and (d) FAES in NaCl solution (500 mg/L Cl<sup>-</sup> and pH 5.9 at 30 °C) with 1.4510 as WE. (e) relative frequency of pits  $RF_{\text{pit}}$  on the stainless steel surface after polarization.

To obtain information about the adsorption and amount of surface coverage, the inhibition efficiency  $\eta$  is calculated [24,25]:

$$\eta = \frac{j_{0,\text{corr}} - j_{s,\text{corr}}}{j_{0,\text{corr}}} \cdot 100 \quad (3)$$

If surfactants adsorb on the stainless steel surface, the corrosion current density measured in a solution with surfactants  $j_{s,\text{corr}}$  should be lower than in a solution without surfactants  $j_{0,\text{corr}}$ . It should be noted that the conductivity increases with increasing surfactant concentration, which is not considered in the formula and thus distorts the efficiency value. It is generally not recommended to use the value calculated by Equation (3) as a quantitative measure of inhibition efficiency if the current densities were derived by Tafel plots because there are many included effects that deviate from the original Tafel theory [26]. Here, inhibition efficiency  $\eta$  is only used as a qualitative parameter for surfactant adsorption. The evaluation of the inhibition efficiency for the LAS and FAES solutions resulted in

0%. Therefore, it can be assumed that LAS, as well as FAES molecules, do not adsorb on the stainless steel surface after immersion. The inhibition efficiency of PKO on the other hand results in  $\eta_{\text{PKO},8x} = 0\%$ ,  $\eta_{\text{PKO},10x} = 37.7\%$ ,  $\eta_{\text{PKO},20x} = 53.9\%$ , and  $\eta_{\text{PKO},40x} = 54.4\%$ , for 8x, 10x, 20x, and 40×CMC, respectively. This suggests that PKO molecules are able to adsorb on the stainless steel surface, forming a protective layer against corrosion processes for concentrations larger than 8×CMC. All corrosion current densities  $j_{\text{corr}}$  are listed in the SI Table S1.

### 3.3. In-Situ AFM

The fact that LAS and FAES increase the breakdown potential (see Figure 4) without increasing the value of inhibition efficiency (Equation (3)) suggests that they adsorb only in the presence of localized corrosion. This mechanism may be called active inhibition, while adsorption of PKO during immersion may represent a passive geometric inhibition. In this section, in-situ AFM measurements are presented to provide a more detailed insight into the inhibition mechanism of the surfactants.

The following results were obtained as described in the measurement methods Section 2.2. Figure 5 shows a representative curve of the current density for the in-situ AFM experiments. Depicted is the current density at different potential differences (vs. Ag/AgCl) for the 1.4510 in the AFM electrochemistry cell, filled with NaCl solution (500 mg/L  $\text{Cl}^-$  and pH 5.9 at 30 °C) with LAS at 16×CMC. For potential differences below the breakdown potential, the current density remains nearly constant. In these cases, the stainless steel was imaged with the AFM while the voltage was applied. However, when the current density increased rapidly over time, the voltage was switched off and the surface was imaged afterwards. Accordingly, as indicated in Figure 5, the surface was imaged up to and including 1600 mV during voltage application and at 1700 and 1800 mV after the voltage was applied.

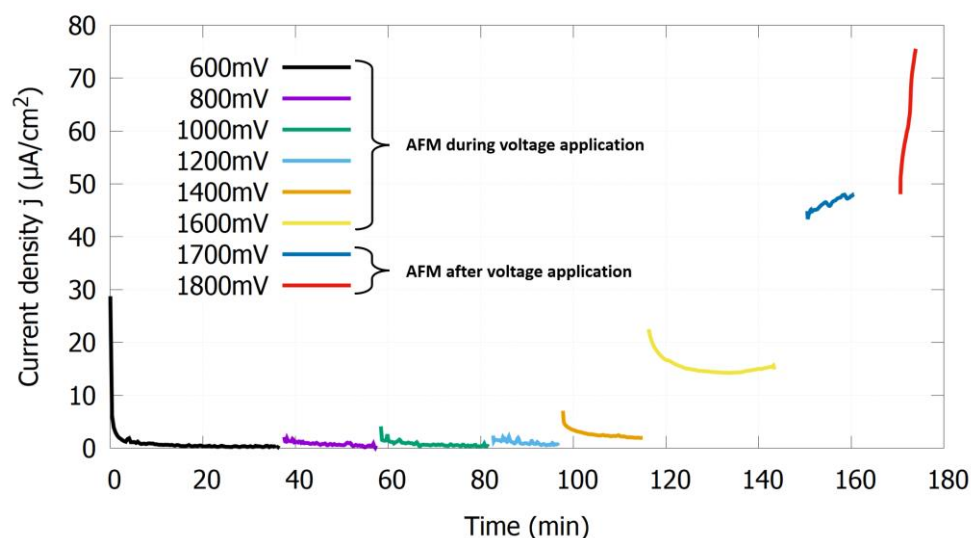


**Figure 5.** Current density over time of the 1.4510 in NaCl solution (500 mg/L  $\text{Cl}^-$  and pH 5.9 at 30 °C) with LAS at 16×CMC in the AFM electrochemical cell at different potential differences vs. Ag/AgCl.

Only after the current density significantly increased at 1800 mV could LAS molecules be identified on the surface in the AFM height images (see Section 3.3.1). Thus, the current density, and hence the number of charge carriers emerging from the surface, is crucial for the adsorption of LAS molecules. It should be noted that only a small portion of the surface can be imaged with AFM, while the measured current density originates from the entire surface. Therefore, it is possible that molecules adsorbed at other locations on the surface, outside the AFM scan area, at lower voltages when the current density was already increased.

With FAES and PKO, there was also no or no additional adsorption on the stainless steel detectable until the current density increased significantly. The current density curves for FAES and PKO follow the same trend as those for LAS. The current remains constant over time until the voltage exceeds the breakdown potential, causing the current to increase significantly (Figures S1–S3). Consequently, the following AFM results show the initial state, i.e., the topography of the 1.4510 surface in the NaCl surfactant solution before any voltage was applied, and the topography after the current density significantly increased.

The results of the potentiodynamic polarization measurements indicated that PKO adsorbs on the steel surface at concentrations higher than  $8\times\text{CMC}$ . Therefore,  $8\times\text{CMC}$  and  $16\times\text{CMC}$  were investigated by in-situ AFM measurements to verify these results and to determine if additional molecules are able to adsorb during potentiostatic measurement. LAS and FAES were also examined at  $16\times\text{CMC}$  for comparison. In addition, the influence of titanium precipitates Ti(C,N) on the adsorption of the surfactants was investigated. The presence of Ti(C,N) was verified by energy dispersive X-ray spectroscopy (EDS) (Figure S4).

### 3.3.1. LAS $16\times\text{CMC}$

Figure 6a shows the 1.4510 surface with a titanium precipitate in NaCl solution ( $500\text{ mg/L Cl}^-$  and pH 5.9 at  $30\text{ }^\circ\text{C}$ ) with LAS at  $16\times\text{CMC}$ . No adsorption of LAS molecules was detectable on the surface after immersion (initial state). Figure 6b depicts the same surface section after local corrosion, caused by a potential difference of 1800 mV until a current density of  $75\text{ }\mu\text{A/cm}^2$  has been reached.

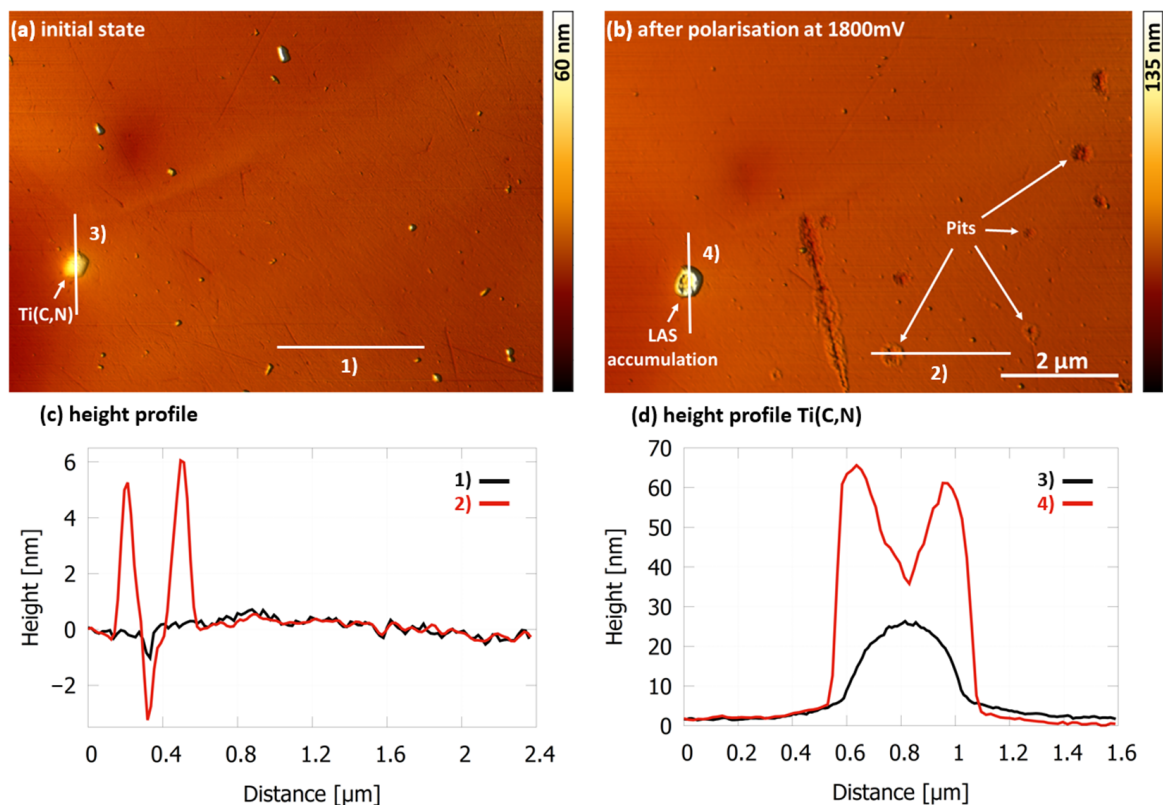


**Figure 6.** AFM height image of 1.4510 steel surface in NaCl solution ( $500\text{ mg/L Cl}^-$  and pH 5.9 at  $30\text{ }^\circ\text{C}$ ) with LAS at  $16\times\text{CMC}$  (a) in the initial state after immersion (0 mV), showing no adsorbed molecules of LAS. (b) After reaching  $75\text{ }\mu\text{A/cm}^2$  at 1800 mV vs. Ag/AgCl, localized adsorption of LAS at pitting initiation sites, especially at the Ti(C,N) can be seen. (c) Height profiles of indicated cross section (1) and (2). (d) Height profiles of the Ti(C,N) at indicated cross section (3) and (4).

The potential difference caused several small pits and a larger pit that follows a defect with protruding fringes, which are most likely adsorbed molecules of LAS. Due to the

very high potential difference achieved here, it should be mentioned that in addition to the chloride attack, further effects such as oxygen evolution also contribute to the dissolution of the surface. Very distinctive is the high coverage of the titanium precipitate by LAS. Since titanium precipitates act as local cathodes [13,27], the ferritic matrix typically dissolves around these precipitates during local corrosion. This explains the ring-shaped accumulation of LAS, which can be clearly seen in Figure 6b,d. However, apart from the areas on the surface where the stainless steel sample has started to dissolve, no further adsorption of LAS can be detected (Figure 6b,c).

### 3.3.2. PKO $8\times$ CMC

In the NaCl solution with PKO at  $8\times$ CMC, no adsorbed molecules could be detected on the surface, as presented in the AFM height image (Figure 7a). Only the bare steel surface can be seen with a titanium carbon-nitride Ti(C,N). Adsorption of surfactants was detectable after the current density reached  $55\ \mu\text{A}/\text{cm}^2$  at 600 mV vs. Ag/AgCl (Figure 7b). The adsorbed molecules present themselves on the surface as relatively evenly distributed small aggregates (white arrows Figure 7b) covering about 2% of the surface. The height profile measured at cross section (2) in Figure 7b shows that PKO adsorbs as a bilayer on the surface. The length of PKO molecules is about 2.1 nm and the height profile results in almost exactly twice this value (Figure 7c).

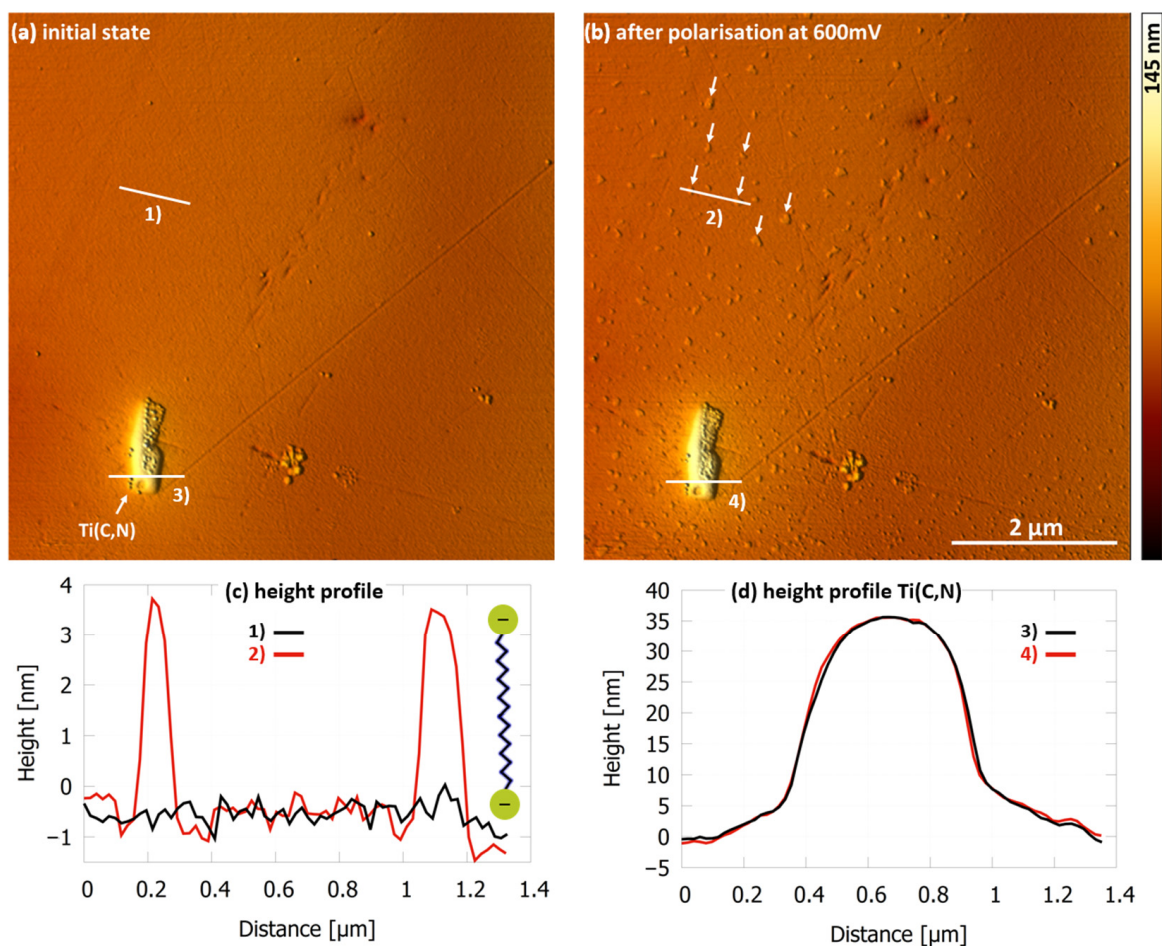


**Figure 7.** AFM height image of 1.4510 steel surface in NaCl solution ( $500\ \text{mg}/\text{L}\ \text{Cl}^-$  and pH 5.9 at  $30\ ^\circ\text{C}$ ) with PKO at  $8\times$ CMC (a) showing no adsorbed molecules on the surface after immersion and (b)  $55\ \mu\text{A}/\text{cm}^2$  at 600 mV vs. Ag/AgCl, PKO adsorbs in small aggregates (white arrows) of bilayer as measured in (c) the height profiles of indicated cross section (1) and (2). (d) Height profiles of the Ti(C,N) at indicated cross section (3) and (4).

There is no preferential adsorption of these molecules at the titanium precipitate detectable (Figure 7a,b,d). The results show that PKO does not adsorb on the surface at and below  $8\times\text{CMC}$  after immersion but adsorbs to a small extent due to the increase in local current density.

### 3.3.3. PKO $16\times\text{CMC}$

If the concentration is increased to  $16\times\text{CMC}$ , PKO already covers large areas of the stainless steel sample after immersion (Figure 8a). The potentiostatic polarization of the stainless steel at  $16\times\text{CMC}$  had the same effect as at  $8\times\text{CMC}$ . No additional adsorption of molecules could be detected as long as the current remained constant over time. But the surface coverage increased by about 8% after the current density increased over time, reaching  $55\ \mu\text{A}/\text{cm}^2$  at 800 mV vs. Ag/AgCl (Figure 8b). Bilayers can be observed again as well as the formation of multilayers as indicated by the height profiles (Figure 8c,d). The formation of these multilayers appears to be energetically more favourable than further lateral expansion to cover additional areas of the stainless steel surface. The preferential multilayer formation could also be observed at higher concentrations (Figure S5).

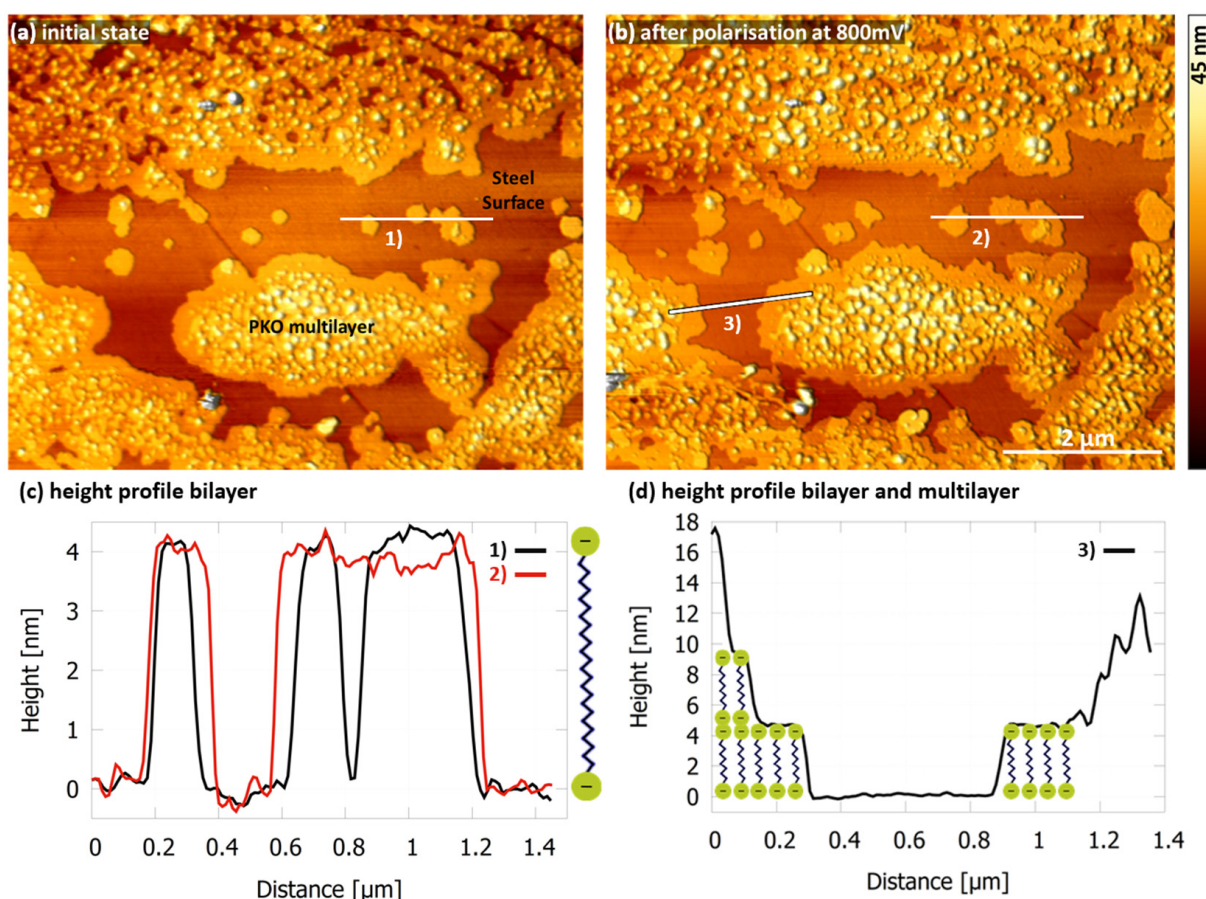


**Figure 8.** AFM height image of 1.4510 surface in NaCl solution ( $500\ \text{mg}/\text{L}\ \text{Cl}^-$  and pH 5.9 at  $30\ ^\circ\text{C}$ ) with PKO at  $16\times\text{CMC}$ . (a) In the initial state after immersion (0 mV) and (b) after a current density of  $55\ \mu\text{A}/\text{cm}^2$  at 800 mV vs. Ag/AgCl was reached showing adsorbed PKO bi- and multilayers on the stainless steel surface with a slightly increased surface coverage. (c) Height profiles of indicated cross section (1) and (2). (d) Height profiles of bilayer and multilayer at the indicated cross section (3).

### 3.3.4. FAES $16\times\text{CMC}$

FAES initially acts like LAS and does not adsorb on the stainless steel surface during immersion as shown in Figure 9a. No FAES molecules could be detected on the ferritic matrix or the titanium precipitate before the current density increased over time at 1400 mV

vs. Ag/AgCl. Figure 9b shows that FAES covers nearly the entire steel surface after switching off the voltage at a current density of  $195 \mu\text{A}/\text{cm}^2$ . A sponge-like structure can be seen on the surface with a few openings, recognizable as indentations, through which the stainless steel sample has only minor contact with the solution. The depth of the indentations is shown in the height profile taken at cross section (2) in Figure 9b. The length of a FAES molecule is about 3 nm and therefore a monolayer has formed here (Figure 9c).

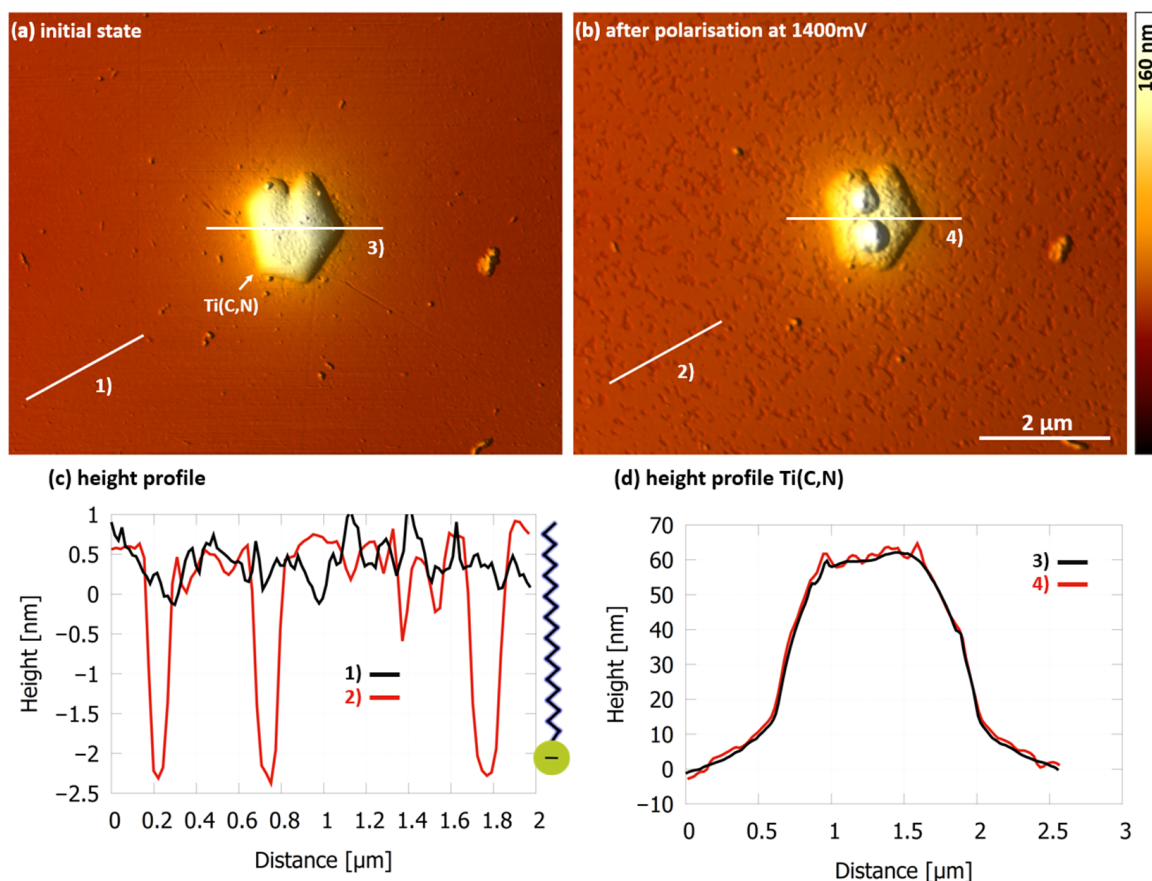


**Figure 9.** (a) AFM height image of 1.4510 surface in NaCl solution ( $500 \text{ mg/L Cl}^-$  and pH 5.9 at  $30^\circ\text{C}$ ) with FAES at  $16\times\text{CMC}$  in the initial state after immersion ( $0 \text{ mV}$ ), showing no adsorbed molecules on the steel surface. (b) Reaching  $195 \mu\text{A}/\text{cm}^2$  at  $1400 \text{ mV}$ , FAES covers nearly the entire surface with a monolayer as indicated by (c) the height profiles of indicated cross section (1) and (2). (d) Height profiles of the Ti(C,N) at the indicated cross section (3) and (4).

A higher current density than before was required until FAES adsorption was detectable. Since only a small portion of the surface can be observed with the AFM, it does not seem unusual that higher currents may also be necessary to trigger local corrosion at the location where the sample is currently imaged. The titanium precipitate in Figure 9b is covered by FAES, which can be recognized by the rougher surface, and is confirmed by the height profiles (Figure 9d). Profile (4) is no longer as smooth as profile (3). Striking are the two elevated accumulations that have formed on the titanium precipitate. However, since the structure of the surface at precisely these two spots was already different than the rest of the precipitate after immersion, it cannot be concluded that titanium precipitates are preferred adsorption sites. The two spots on the precipitate could be residues from the sample preparation, which have caused preferential adsorption at these spots. Nonetheless, FAES shows a promising inhibition mechanism with the monolayer surface coverage when localized corrosion occurs. Thus, nucleation at the surface seems to be necessary for further molecules to subsequently accumulate at the surface, and these nucleation sites are caused by the breakdown of the passive layer.

### 3.4. Summary

The surface tension measurements revealed a significantly lower CMC for PKO (0.013 g/L) compared to FAES (0.17 g/L) and LAS (0.45 g/L). The low CMC and thus good aggregation ability enables PKO to adsorb on the 1.4510 surface for concentrations greater than  $8\times\text{CMC}$  during immersion. This was shown by both the electrochemical polarization and the in-situ AFM measurements. The surface coverage and inhibition effect of PKO reached a maximum at  $20\times\text{CMC}$  with a breakdown potential  $E_{\text{bd}}$  of about 1070 mV. The adsorption occurred and was randomly distributed over the surface, and no domains could be identified with increased accumulation. Therefore, possible pitting initiation sites on the surface are also covered purely randomly. This could explain the large standard deviations of the  $E_{\text{bd}}$  in the potentiodynamic polarization measurements. During the polarization of the 1.4510, PKO molecules can adsorb on the surface as the current density increases over time. Therefore, even at and below  $8\times\text{CMC}$ , higher  $E_{\text{bd}}$  are achieved than without PKO in the NaCl solution. In general, no monolayer formation could be detected for PKO, only bilayer or multilayer were present.

LAS does not adsorb on the stainless steel surface during immersion, as suggested by the potentiodynamic polarization measurement and confirmed by the in-situ AFM measurements. LAS agglomerates were found exclusively at pitting sites on the surface after local corrosion. Therefore, LAS blocks only active sites on the 1.4510 and is not able to form a protective layer on the surface. However, the pitting initiation sites are inhibited very effectively, and thus further pit propagation is prevented. A limit value in the  $E_{\text{bd}}$  with approximately 1210 mV is already reached at  $8\times\text{CMC}$ . This means that the breakdown potential of the 1.4510 has been tripled.

FAES adsorbed only on the surface after an increase in current was measured, just like LAS. However, it does not form local aggregates but forms a monolayer on the surface with only a few defects. The breakdown potentials of FAES determined by the potentiodynamic measurements are very similar to those of LAS and are above a concentration of  $16\times\text{CMC}$  on average 1220 mV.

Since titanium precipitates can act as local cathodes [13,27] they are potential pitting initiation sites. Unfortunately, all three surfactants investigated did not show preferential adsorption on titanium precipitates of the 1.4510 stainless steel after immersion.

## 4. Discussion

In this study we investigated how anionic surfactants inhibit the corrosion of a stainless steel sample and thus it represents application-oriented research for household appliances. The inhibition effect of surfactants on ferritic stainless steel in near neutral sodium chloride solution, in particular the underlying mechanism, has rarely been studied to date.

The electrochemical polarization measurements at various concentrations have revealed that the anionic surfactants inhibit pitting corrosion effectively but to varying degrees. With LAS concentrations between  $1\times$  and  $4\times\text{CMC}$ , the breakdown potential  $E_{\text{bd}}$  ranges around 800 mV. Upon reaching a concentration of  $8\times\text{CMC}$ , a threshold value of approximately 1210 mV is attained, beyond which the  $E_{\text{bd}}$  does not increase further. Only a small increase in  $E_{\text{bd}}$  is observed at the highest concentration of  $160\times\text{CMC}$ . Light microscopic analysis of the stainless steel has shown a reduction in the number of pits on the surface up to  $4\times\text{CMC}$ . Up to this concentration, the increase of surfactant molecules in the solution enhances the inhibition of pitting corrosion. Above this concentration, an adequate number of molecules seem to be consistently present in the vicinity of a potential initiation site to adsorb in sufficient quantities when pitting corrosion occurs, thereby inhibiting the exchange with the solvent. However, the exact underlying binding process must be clarified in further studies. Upon exceeding this concentration, an increase in crevice corrosion occurs, as pitting corrosion is effectively prevented. The adsorption of surfactants in the crevice is presumably hindered by spatial constriction. The FAES exhibits a very similar behavior. From  $2\times$  to  $8\times\text{CMC}$ , the  $E_{\text{bd}}$  is on average 785 mV. Up to  $8\times\text{CMC}$ , light microscopy analysis following electrochemical polarization shows a decrease in the

occurrence of pits on the surface. Therefore, a higher concentration of FAES compared to LAS is required to efficiently suppress pitting corrosion, leading to increased crevice corrosion. However, for  $16\times\text{CMC}$  and higher concentrations, comparable  $E_{\text{bd}}$  values (1220 mV on average) are achieved as with LAS for  $8\times\text{CMC}$  and higher concentrations. The  $E_{\text{bd}}$  increases with increasing concentration of PKO in the solution up to  $20\times\text{CMC}$ . Different threshold concentrations are therefore achieved for the three surfactants, which can be specified as a practical value, above which the inhibitory effect does not increase any further. This is  $8\times\text{CMC}$  for LAS,  $16\times\text{CMC}$  for FAES, and  $20\times\text{CMC}$  for PKO. With PKO, the  $E_{\text{bd}}$  value above  $20\times\text{CMC}$  is on average 1070 mV. Consequently, it exhibits a poorer inhibitory effect compared to LAS or FAES. This is corroborated by the light microscopy analysis, as at comparable concentrations, pits on the surface occur more frequently than with LAS and FAES, thereby demonstrating less effective inhibition. This occurs because PKO molecules cover the surface in a randomly distributed manner and at higher concentrations, they tend to form multilayers before achieving full coverage of the stainless steel surface. Consequently, potential pitting sites are also randomly covered. In the event of pitting corrosion, PKO molecules exhibit less effective adsorption to initiation sites compared to LAS or FAES, which ultimately leads to the lowest inhibition effect among the three surfactants investigated.

Yalcinkaya et al. [20] investigated PKO, LAS, and FAES using electrochemical measurement techniques in a research project preceding this work. Here, it was already assumed that PKO can adsorb on the stainless steel surface and that LAS and FAES only interact with pitting initiation sites. In this study, we could verify the different inhibition mechanisms and analyse them in much more detail using the demonstrated in-situ AFM technique. It has been shown that the inhibition efficiency  $\eta$  frequently used in literature (Equation (3)) [12] allows conclusions to be drawn about the quantity of molecules adsorbed on the stainless steel surface; it does not, however, adequately describe the inhibition efficiency of all surfactants. The inhibition efficiency  $\eta$  is calculated from the decrease in the corrosion current density that occurs when inhibitors accumulate on the steel surface. As shown for LAS and FAES, there is no surfactant adsorption on the surface during immersion and therefore no decrease in the corrosion current density. Nevertheless, these surfactants exhibit excellent corrosion-inhibiting properties.

Interestingly, adsorption at  $1\times\text{CMC}$  was generally not measurable. Typically, adsorption of surfactants is expected to be possible below  $1\times\text{CMC}$  and the formation of bi- or multilayers begins above  $1\times\text{CMC}$  [17,18,28]. The formation of micelles in the solution thus appears initially to be energetically more favourable than adsorption on the stainless steel surface, even for PKO. One reason may be that the polished surface of the 1.4510 presented a hydrophobic character, making adsorption generally less favourable for surfactants with their hydrophilic head group. Since PKO always adsorbed at least as bilayers on the surface and no monolayers could be detected, it is possible that the micelles accumulate directly on the surface and are then supplemented by other molecules. The rather low adsorption affinity to the surface is also evident at higher concentrations due to the rapid formation of multilayers, so that ultimately only about half of the surface was covered with PKO.

Wei et al. [29] demonstrated that surface coverage of surfactants alone is not sufficient to obtain pitting inhibition. They investigated nonionic, cationic, and anionic surfactants as corrosion inhibitors of a 1.4301 stainless steel in NaCl solution. Although the non-ionic and cationic surfactants covered the surface with a monolayer, no inhibitory effects have been observed. Only the anionic surfactant, in this case a sodium dodecylsulfate (SDS), was able to inhibit the pitting corrosion. SDS has a similar molecular structure to FAES. Wei et al. [29] argued that SDS possibly adsorbs on the same surface sites, as do chloride ions, because they are both negatively charged, and the resulting electrostatic repulsion keeps chloride ions off the surface. Interestingly, complete surface coverage of the 1.4301 could not be achieved with SDS, as we observed with PKO on the 1.4510. Nevertheless, Wei et al. reported complete pitting inhibition even at half monolayer coverage and concluded that SDS adsorbs preferentially at pitting initiation sites. However, it may also be possible that

SDS initially adsorbs randomly distributed on the surface and additional SDS molecules adsorb when localized corrosion occurs, as we were able to demonstrate for FAES and LAS on the 1.4510. Of course, the molecules still adsorb preferentially at pitting sites, but whether they do this during immersion or only when local corrosion occurs is crucial for a better understanding of the inhibition mechanism.

Wei et al. [28] reported in another well-founded study that N-lauroylsarcosine, an anionic surfactant with a carboxy group like PKO, can adsorb on 1.4301 stainless steel in NaCl during immersion. Monolayer adsorption was measured at a concentration of  $1 \times \text{CMC}$  and the formation of bilayers at higher concentrations. Interestingly, Wei et al. [28] reported that at least a monolayer coverage was necessary to obtain an increase in pitting potential. The three surfactants investigated in this study caused an increase in pitting potential, even if no molecules were adsorbed on the 1.4510 surface after immersion. It remains to be elucidated under which conditions anionic surfactants provide pitting inhibition only by homogeneous surface blocking or by blocking active sites during localized corrosion.

The head group of a surfactant determines its properties; the electron density at the reaction center is especially important for chemisorption [9,17,30]. It is reported that a higher electron density near the reaction center can improve the chemisorption [17,30]. In this case, LAS and FAES with the sulfonate and sulfate group should have an advantage over PKO with the carboxyl group. Therefore, we assume that during the immersion, no adsorption by chemisorption is possible. Otherwise, adsorption of LAS or FAES molecules would have been detectable prior to localized corrosion, as with PKO. PKO probably does adsorb initially by physisorption promoted by the high aggregation ability and surface activity resulting from its low CMC. However, LAS and FAES can be detected on the surface after the current density increased during potentiostatic polarization. Therefore, LAS and FAES may favorably adsorb by chemisorption when corresponding binding sites are exposed by local corrosion. In addition, the breakdown of the passive layer during localized corrosion causes positively charged ions to emerge from the surface. These should attract the anionic surfactants, resulting in an accumulation at the initiation sites, which should promote especially chemisorption.

## 5. Conclusions

In-situ AFM measurements during potentiostatic polarization measurement provide deep insights into the active inhibition mechanism of selected inhibitors. Preferred adsorption sites on the stainless steel surface, such as precipitates, can be identified and the accumulation of surfactants on the surface can be characterized. Thus, it was shown that the action of surfactants on stainless steel can deviate from the homogeneous surface blocking one would normally expect. Accordingly, no monolayer has formed on the surface at  $1 \times \text{CMC}$  and there are surfactants that do not adsorb on the surface after immersion, but they provide their protective activity when local corrosion initiates. However, the existing measuring method currently lacks the capability to image the entire steel surface during polarization. Therefore, the measured current density cannot be directly correlated with the AFM images.

The three anionic surfactants investigated in this study demonstrated a very good inhibition, effectively protecting the stainless steel from pitting corrosion. Nevertheless, LAS and FAES provide better corrosion inhibiting properties than PKO. PKO achieves efficient geometric inhibition by randomly distributed surface coverage of bi- or multilayer. LAS and FAES favourably adsorb only when corresponding binding sites are exposed by local corrosion. As such, FAES forms a monolayer on the surface and LAS accumulates only at pitting initiation sites. During immersion, generally no preferential adsorption on the titanium precipitates was detectable. Although we have successfully identified the distinct adsorption mechanisms of the three surfactants, further clarification is needed regarding the precise binding process, especially for LAS and FAES.

Our results prove that in-situ AFM can be used to gain deep insights into the mechanism of real corrosion processes, allowing the development of tailored and more efficient

corrosion inhibitors for technical applications. The gain in corrosion resistance and prolongation of the product lifecycle is believed to be as one the major impacts towards more reliable and durable products for a sustainable future.

**Supplementary Materials:** The following supporting information can be downloaded at: <https://www.mdpi.com/article/10.3390/cmd5020009/s1>, Figure S1: Current density over time of the 1.4510 in NaCl solution (500 mg/L Cl<sup>-</sup> and pH 5.9 at 30 °C) with FAES at 16×CMC in the AFM electrochemical cell at different potential differences vs. Ag/AgCl; Figure S2: Current density over time of the 1.4510 in NaCl solution (500 mg/L Cl<sup>-</sup> and pH 5.9 at 30 °C) with PKO at 16×CMC in the AFM electrochemical cell at different potential differences vs. Ag/AgCl; Figure S3: Current density over time of the 1.4510 in NaCl solution (500 mg/L Cl<sup>-</sup> and pH 5.9 at 30 °C) with PKO at 8×CMC in the AFM electrochemical cell at different potential differences vs. Ag/AgCl; Figure S4: SEM image of the polished 1.4510 with titanium precipitated. EDS spectra present the percentage composition of the steel matrix (S1) and two titanium nitride precipitates (S2,S3); Figure S5: AFM height image of 1.4510 steel surface in NaCl solution (500 mg/L Cl<sup>-</sup> and pH 5.9 at 30 °C) with PKO at 20×CMC after immersion showing multilayer formation; Table S1: Corrosion current densities  $j_{\text{corr}}$  of the 1.4510 stainless steel, without surfactants 0×CMC and with increasing concentration of FAES, LAS and PKO in NaCl solution (500 mg/L Cl<sup>-</sup> and pH 5.9 at 30 °C).

**Author Contributions:** Conceptualization: T.K., A.H. and D.A.; Methodology: J.C., S.K., H.J.K., A.G., K.R., T.K., A.H. and D.A.; Validation: J.C., S.K., T.K., A.H. and D.A.; Investigation: J.C., S.K. and H.J.K.; Resources: A.G., K.R., T.K., A.H. and D.A.; Writing—original draft: J.C.; Writing—review and editing: S.K., H.J.K., A.G., K.R., T.K., A.H. and D.A.; Visualization: J.C.; Supervision: T.K., A.H. and D.A.; Funding acquisition: T.K., A.H. and D.A. All authors have read and agreed to the published version of the manuscript.

**Funding:** This research was funded by grants from the State of North Rhine–Westphalia using funds from the European Regional Development Fund (EFRE) (EFRE-1803FI12), the Center for Interdisciplinary Material Research and Technology Development (CiMT) and from the University of Bielefeld.

**Data Availability Statement:** The data that support the findings of this study are available from the corresponding author upon reasonable request.

**Acknowledgments:** We thank Michaela Klöcker for the support with the SEM measurements.

**Conflicts of Interest:** Authors Alix Gaspard and Karsten Rasim were employed by the company Miele & Cie. KG. The remaining authors declare that the research was conducted in the absence of any commercial or financial relationships that could be construed as a potential conflict of interest.

## References

1. Javaherdashti, R. How Corrosion Affects Industry and Life. *Anti-Corros. Methods Mater.* **2000**, *47*, 30–34. [[CrossRef](#)]
2. Thompson, N.G.; Yunovich, M.; Dunmire, D. Cost of Corrosion and Corrosion Maintenance Strategies. *Corros. Rev.* **2007**, *25*, 247–262. [[CrossRef](#)]
3. McBee, C.L.; Kruger, J. Nature of Passive Films on Iron-Chromium Alloys. *Electrochim. Acta* **1972**, *17*, 1337–1341. [[CrossRef](#)]
4. Zaffora, A.; Di Franco, F.; Santamaria, M. Corrosion of Stainless Steel in Food and Pharmaceutical Industry. *Curr. Opin. Electrochem.* **2021**, *29*, 100760. [[CrossRef](#)]
5. Elsener, B.; Fantauzzi, M.; Rossi, A. Stainless Steels: Passive Film Composition, Pitting Potentials, and Critical Chloride Content in Concrete. *Mater. Corros.* **2020**, *71*, 797–807. [[CrossRef](#)]
6. Frankel, G.S. Pitting Corrosion of Metals: A Review of the Critical Factors. *J. Electrochem. Soc.* **1998**, *145*, 2186–2198. [[CrossRef](#)]
7. Sanni, O.; Sunday Isaac Fayomi, O.; Patricia Idowu Popoola, A. Eco-Friendly Inhibitors for Corrosion Protection of Stainless Steel: An Overview. *J. Phys. Conf. Ser.* **2019**, *1378*, 042047. [[CrossRef](#)]
8. Ma, I.A.W.; Ammar, S.; Kumar, S.S.A.; Ramesh, K.; Ramesh, S. A Concise Review on Corrosion Inhibitors: Types, Mechanisms and Electrochemical Evaluation Studies. *J. Coat. Technol. Res.* **2022**, *19*, 241–268. [[CrossRef](#)]
9. Taghavikish, M.; Dutta, N.K.; Choudhury, N.R. Emerging Corrosion Inhibitors for Interfacial Coating. *Coatings* **2017**, *7*, 217. [[CrossRef](#)]
10. Pourbaix, M. Applications of Electrochemistry in Corrosion Science and in Practice. *Corros. Sci.* **1974**, *14*, 25–82. [[CrossRef](#)]
11. Wang, S.; Zhang, J.; Gharbi, O.; Vivier, V.; Gao, M.; Orazem, M.E. Electrochemical Impedance Spectroscopy. *Nat. Rev. Methods Primers* **2021**, *1*, 41. [[CrossRef](#)]

12. Chan, K.W.; Tjong, S.C. Effect of Secondary Phase Precipitation on the Corrosion Behavior of Duplex Stainless Steels. *Materials* **2014**, *7*, 5268–5304. [[CrossRef](#)]
13. Hou, Y.; Nakamori, Y.; Kadoi, K.; Inoue, H.; Baba, H. Initiation Mechanism of Pitting Corrosion in Weld Heat Affected Zone of Duplex Stainless Steel. *Corros. Sci.* **2022**, *201*, 110278. [[CrossRef](#)]
14. Kiremit, S.; Cremer, J.; Stallmeier, Y.; Sonntag, A.; Klöcker, M.; Anselmetti, D.; Hütten, A.; Kordisch, T. Development of an In Situ Micro-Corrosion Cell for the Investigation of Pitting Corrosion on Austenitic and Ferritic Stainless Steels. *Corros. Mater. Degrad.* **2023**, *4*, 104–119. [[CrossRef](#)]
15. Smulders, E.; von Rybinski, W.; Sung, E.; Rähse, W.; Steber, J.; Wiebel, F.; Nordskog, A. Laundry Detergents. In *Ullmann's Encyclopedia of Industrial Chemistry*; John Wiley & Sons: Hoboken, NJ, USA, 2007. [[CrossRef](#)]
16. Fiori-Bimbi, M.V.; Alvarez, P.E.; Vaca, H.; Gervasi, C.A. Corrosion Inhibition of Mild Steel in HCL Solution by Pectin. *Corros. Sci.* **2015**, *92*, 192–199. [[CrossRef](#)]
17. Malik, M.A.; Hashim, M.A.; Nabi, F.; AL-Thabaiti, S.A.; Khan, Z. Anti-Corrosion Ability of Surfactants: A Review. *Int. J. Electrochem. Sci.* **2011**, *6*, 1927–1948. [[CrossRef](#)]
18. Free, M.L.; Wang, W.; Ryu, D.Y. Prediction of Corrosion Inhibition Using Surfactants. *Corrosion* **2004**, *60*, 837–844. [[CrossRef](#)]
19. Tobsin, T.; Bangchit, P.; Sirikullertrat, V.; Sutthiruangwong, S. Influence of Sodium Dodecyl Sulfate on Corrosion Behavior of 304 Stainless Steel. *Thammasat Int. J. Sci. Technol.* **2010**, *15*, 40–46.
20. Yalcinkaya, M.O.; Gaspard, A.; Altenbach, C.; Zander, D. Effect of Anionic Surfactants as Pitting Corrosion Inhibitors for Stainless Steels. *Mater. Corros.* **2023**, *74*, 1196–1207. [[CrossRef](#)]
21. Kiremit, S. *Analyse des Korrosionsverhaltens Ferritischer und Austenitischer Nichtrostender Stähle in Wässrigen Elektrolyten unter Verwendung Einer In-Situ Mikrokorrosionszelle*; Universität Bielefeld: Bielefeld, Germany, 2023.
22. Nečas, D.; Klapetek, P. Gwyddion: An Open-Source Software for SPM Data Analysis. *Cent. Eur. J. Phys.* **2012**, *10*, 181–188. [[CrossRef](#)]
23. Hiemenz, P.C.; Rajagopalan, R. *Principles of Colloid and Surface Chemistry*, 3rd ed.; Marcel Dekker, Inc.: New York, NY, USA, 1997; ISBN 0-8247-9397-8.
24. Sherif, E.M.; Park, S.M. Effects of 2-Amino-5-Ethylthio-1,3,4-Thiadiazole on Copper Corrosion as a Corrosion Inhibitor in Aerated Acidic Pickling Solutions. *Electrochim. Acta* **2006**, *51*, 6556–6562. [[CrossRef](#)]
25. Migahed, M.A.; Azzam, E.M.S.; Al-Sabagh, A.M. Corrosion Inhibition of Mild Steel in 1 M Sulfuric Acid Solution Using Anionic Surfactant. *Mater. Chem. Phys.* **2004**, *85*, 273–279. [[CrossRef](#)]
26. Finšgar, M.; Jackson, J. Application of Corrosion Inhibitors for Steels in Acidic Media for the Oil and Gas Industry: A Review. *Corros. Sci.* **2014**, *86*, 17–41. [[CrossRef](#)]
27. Tiarniyu, A.A.; Eduok, U.; Szpunar, J.A.; Odeshi, A.G. Corrosion Behavior of Metastable AISI 321 Austenitic Stainless Steel: Investigating the Effect of Grain Size and Prior Plastic Deformation on Its Degradation Pattern in Saline Media. *Sci. Rep.* **2019**, *9*, 12116. [[CrossRef](#)]
28. Wei, Z.; Duby, P.; Somasundaran, P. Pitting Inhibition of Stainless Steel by Surfactants: An Electrochemical and Surface Chemical Approach. *J. Colloid. Interface Sci.* **2003**, *259*, 97–102. [[CrossRef](#)]
29. Wei, Z.; Somasundaran, P.; Duby, P. Pitting Inhibition by Surfactants. *J. Electrochem. Soc.* **2004**, *151*, B304. [[CrossRef](#)]
30. El-Maksoud, S.A.A. The Effect of Organic Compounds on the Electrochemical Behaviour of Steel in Acidic Media. A Review. *Int. J. Electrochem. Sci.* **2008**, *3*, 528–555. [[CrossRef](#)]

**Disclaimer/Publisher's Note:** The statements, opinions and data contained in all publications are solely those of the individual author(s) and contributor(s) and not of MDPI and/or the editor(s). MDPI and/or the editor(s) disclaim responsibility for any injury to people or property resulting from any ideas, methods, instructions or products referred to in the content.